

RESEARCH ARTICLE

Cerebellar, Not Nigrostriatal Degeneration Impairs Dexterity in Multiple System Atrophy

Alexander Rau, MD,^{1,2} Jonas A. Hosp, MD,³ Michel Rijntjes, MD,³ Cornelius Weiller, MD,³ Elias Kellner, PhD,⁴ Emir Berberovic, MD,⁵ Panteleimon Oikonomou, MD,⁵ Wolfgang H. Jost, MD,⁵ Marco Reisert, PhD,^{4,6} Horst Urbach, MD,¹ and Nils Schröter, MD^{3*}

¹Department of Neuroradiology, Medical Center—University of Freiburg, Faculty of Medicine, University of Freiburg, Freiburg, Germany

²Department of Diagnostic and Interventional Radiology, Medical Center—University of Freiburg, Faculty of Medicine, University of Freiburg, Freiburg, Germany

³Department of Neurology and Clinical Neuroscience, Medical Center—University of Freiburg, Faculty of Medicine, University of Freiburg, Freiburg, Germany

⁴Medical Physics, Department of Diagnostic and Interventional Radiology, Medical Center—University of Freiburg, Faculty of Medicine, University of Freiburg, Freiburg, Germany

⁵Parkinson-Klinik Ortenau, Wolfach, Germany

⁶Department of Stereotactic and Functional Neurosurgery, Medical Center—University of Freiburg, Faculty of Medicine, University of Freiburg, Freiburg, Germany

ABSTRACT: Background: Multiple system atrophy (MSA) clinically manifests with either predominant nigrostriatal or cerebellopontine degeneration. This corresponds to two different phenotypes, one with predominant Parkinson's symptoms (MSA-P [multiple system atrophy-parkinsonian subtype]) and one with predominant cerebellar deficits (MSA-C [multiple system atrophy-cerebellar subtype]). Both nigrostriatal and cerebellar degeneration can lead to impaired dexterity, which is a frequent cause of disability in MSA.

Objective: The aim was to disentangle the contribution of nigrostriatal and cerebellar degeneration to impaired dexterity in both subtypes of MSA.

Methods: We thus investigated nigrostriatal and cerebellopontine integrity using diffusion microstructure imaging in 47 patients with MSA-P and 17 patients with MSA-C compared to 31 healthy controls (HC). Dexterity was assessed using the 9-Hole Peg Board (9HPB) performance.

Results: Nigrostriatal degeneration, represented by the loss of cells and neurites, leading to a larger free-fluid compartment, was present in MSA-P and MSA-C when

compared to HCs. Whereas no intergroup differences were observed between the MSAs in the substantia nigra, MSA-P showed more pronounced putaminal degeneration than MSA-C. In contrast, a cerebellopontine axonal degeneration was observed in MSA-P and MSA-C, with stronger effects in MSA-C. Interestingly, the degeneration of cerebellopontine fibers is associated with impaired dexterity in both subtypes, whereas no association was observed with nigrostriatal degeneration.

Conclusion: Cerebellar dysfunction contributes to impaired dexterity not only in MSA-C but also in MSA-P and may be a promising biomarker for disease staging. In contrast, no significant association was observed with nigrostriatal dysfunction. © 2023 The Authors. *Movement Disorders* published by Wiley Periodicals LLC on behalf of International Parkinson and Movement Disorder Society.

Key Words: multiple system atrophy; diffusion multicompartiment imaging; diffusion microstructure imaging; substantia nigra; putamen; dexterity; cerebellar dysfunction

This is an open access article under the terms of the [Creative Commons Attribution-NonCommercial-NoDerivs](#) License, which permits use and distribution in any medium, provided the original work is properly cited, the use is non-commercial and no modifications or adaptations are made.

*Correspondence to: Dr. Nils Schröter, Department of Neurology and Clinical Neuroscience, Medical Center—University of Freiburg, Faculty of Medicine University of Freiburg, Breisacher Str. 64, 79106 Freiburg, Germany; E-mail: nils.schroeter@uniklinik-freiburg.de

Funding agency: This study was funded by Berta-Ottenstein-Programme for Clinician Scientists, Faculty of Medicine, University of Freiburg.

Relevant conflicts of interest/financial disclosures: The authors have nothing to disclose. The authors declare no competing nonfinancial or financial interests.

Received: 13 July 2023; **Accepted:** 30 October 2023

Published online 27 November 2023 in Wiley Online Library (wileyonlinelibrary.com). DOI: 10.1002/mds.29661

Multiple system atrophy (MSA) is an atypical Parkinson's syndrome that manifests with hypokinetic-rigid symptoms, cerebellar dysfunction, and autonomic failure, with two clinical subtypes presenting with either a predominant Parkinson's (MSA-P [multiple system atrophy-parkinsonian subtype]) or cerebellar (MSA-C [multiple system atrophy-cerebellar subtype]) syndrome.¹

In MSA, pronounced neuronal cellular degeneration is present in the putamen and substantia nigra (SN), whereas widespread gliosis is observed with an accentuation in the olivary nucleus, cerebellum, and SN.² Pathological hallmarks are glial cytoplasmic inclusions, containing aggregations of α -synuclein, that are observed with a nigrostriatal and olivopontocerebellar emphasis.²⁻⁴

Whereas widespread neurodegeneration is observed in both MSA subtypes, a nigrostriatal accentuation is associated with the MSA-P subtype, and a more pronounced degeneration in the olivary nucleus and in the cerebellar cortex, dentate nucleus, and interconnecting white matter (WM) (ie, the middle cerebellar peduncle [MCP] and pontine crossing tracts [PCT]) is associated with MSA-C.² MSA-P and MSA-C are thought to comprise a continuum of the same entity, and frequently an overlapping symptomatology is observed.¹ Whereas MSA-P is about two to four times more common than MSA-C in Europe, a greater proportion of MSA-C is found in Japan.⁴ Patients with MSA-P initially present with rigidity followed by tremor, bradykinesia, and postural instability. In contrast, patients with MSA-C first develop dysarthria and ataxia. Autonomic deficits are observed early in the course of both subtypes, sometimes already as initial clinical manifestation.⁵ With disease progression, these deficits lead to impairment in almost all areas of daily activity with a substantial reduction in quality of life.⁶ Impaired dexterity is often present in both MSA subtypes and contributes to the loss of independency in activities of daily living, such as cutting food or dressing.⁷ Furthermore, it is directly associated with impaired quality of life in other disorders like neuropathies.⁸ However, the underlying cause of the reduced dexterity is unclear as cerebellar, extra-pyramidal motor, and pyramidal tract changes may contribute and all structures are affected in MSA.^{9,10}

A great challenge is posed by the clinical weighting of individual deficits as well as by the differentiated attribution of regionally accentuated neurodegeneration patterns. Here, the microstructure is of particular interest, because changes at this level precede the macrostructural alteration, as already demonstrated in other neurodegenerative disorders such as Parkinson's disease (PD).¹¹⁻¹³

Diffusion-based magnetic resonance imaging (dMRI) is a promising technique to study microstructural alterations of the brain in vivo and noninvasively. The

microstructural composition can be approximated by mesoscopically distinguishing between different anatomical compartments based on their diffusion properties.¹⁴ The basis for this is that the movement of "free" water molecules is random and unrestricted, whereas water molecules in neuronal processes or the extracellular matrix are aligned by organelles and membranes. Biophysically motivated diffusion microstructure imaging (DMI)¹⁵ offers more specific measures of tissue integrity than classical diffusion tensor imaging and is more suited to detect pathological conditions than neurite orientation dispersion and density imaging (NODDI).¹⁴ For this, DMI relies on the standard model¹⁴⁻¹⁶ which comprises three compartments that differ in their diffusion properties defined by membrane boundaries: the free water/CSF fraction (V-CSF) accounting for the cerebrospinal fluid and perivascular spaces; the intra-axonal volume fraction (V-intra) with one-dimensional diffusion within tight membrane borders; and the extra-axonal volume fraction (V-extra) corresponding to the extra-axonal cellular compartment and the extracellular matrix, characterized by restricted diffusion. This approach thus allows for disentangling the microstructure from the effects of macroscopic tissue geometry such as fiber crossings. DMI has been applied in recent studies and detects degenerating neuronal somata and loss in the extracellular matrix by a decrease in the parameter "V-extra," whereas degenerating dendrites and myelinated axons are detected through a decrease in "V-intra." Moreover, an increase in free interstitial fluid (resulting from the loss of both axons and cell bodies or inflammation) leads to an elevated "V-CSF."¹⁷⁻²⁰

This study employed DMI to¹ elucidate microstructural correlates of the distinct clinical phenotypes of MSA-P and MSA-C and to² disentangle the contribution of nigrostriatal and cerebellopontine degeneration to impaired dexterity in MSA-P and MSA-C.

Patients and Methods

Study Participants and Clinical Outcomes

This retrospective analysis included DMI data from (1) 64 consecutive patients with MSA (47 MSA-P, 17 MSA-C) who received routine MRI in a 5-year period between February 2018 and February 2023 for the differential diagnosis of a Parkinson's syndrome and (2) 31 healthy controls (HC). The study was approved by the Institutional Review Board (Ethics Committee—University of Freiburg, EK 400/20) and carried out in accordance with the Declaration of Helsinki and its later amendments. Due to the retrospective nature of this study, the need for written informed consent was waived. The study protocol is summarized in Figure 1.

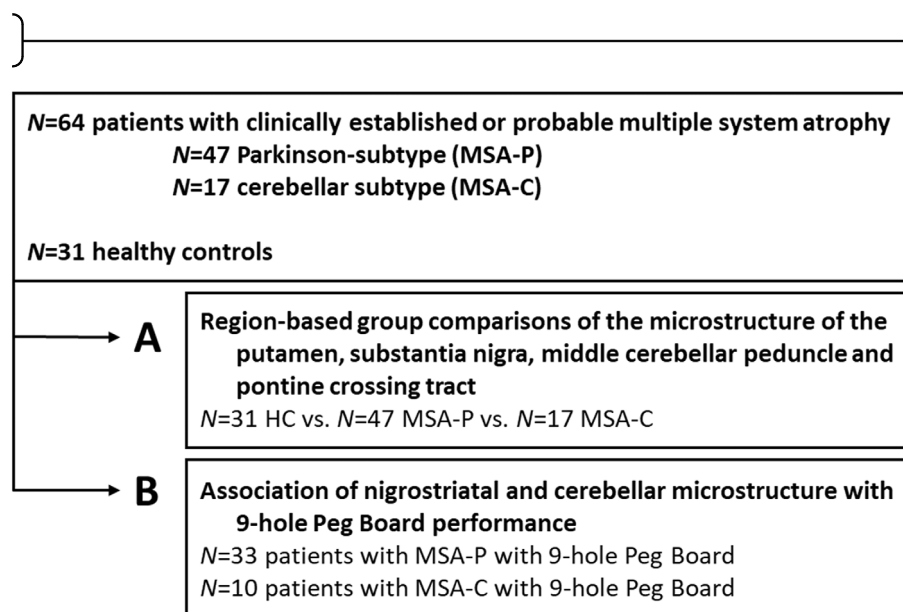


FIG. 1. Study protocol and group allocation of patients. MSA-P, multiple system atrophy-parkinsonian subtype; MSA-C, multiple system atrophy-cerebellar subtype; HC, healthy controls.

Inclusion criteria were the diagnosis of a clinically established or highly probable MSA and dMRI, acquired between February 2018 and February 2023. Corrupted image data served as exclusion criteria. Clinical diagnoses were retrospectively validated by experts in movement disorders (M.R. and W.H.J., board-certified neurologists; NS, >8 years of neurology training) based on current diagnostic criteria.¹ All available medical records were used for consensus diagnosis on a case-by-case basis. Imaging data indicative of MSA were available in the form of ¹⁸fluorodeoxyglucose-positron emission tomography (FDG-PET) data in all patients.²¹ Additionally, findings from DaTSCAN, residual urine measurements, orthostatic tests, and, in a subset, the results of a levodopa challenge were also taken into account. Results from neuropsychological screening examinations were also considered. According to current consensus criteria, the classification of patients into their respective subtypes (MSA-P or MSA-C) was based on the predominant motor syndrome. In patients with a predominant hypokinetic-rigid syndrome, MSA-P was diagnosed. In patients with predominant cerebellar deficits such as ataxia, the diagnosis of MSA-C was made.

Dexterity was assessed in 33 patients with MSA-P and 10 patients with MSA-C in a standardized manner using the 9-Hole Peg Board (9HPB) performance (once per hand), resembled by the mean time to solve the 9HPB between both sides.²² The age- and sex-adjusted norm values were adapted from Oxford et al. The mean value was calculated by averaging the norm values from the left and the right hands. Patients were classified as pathological when their performance in the 9HPB was at least two standard deviations above the age- and sex-specific norm (Table 2).²³

Subjects in the HC group had no known neurological medical condition, no neurological deficits on clinical examination, and no family history of neurodegenerative disorders.

Brain MRI Acquisition

MRI was performed using a 3-T scanner (MAGNETOM Prisma, Siemens Healthcare, Erlangen, Germany) with a 64-channel head and neck coil. T1-weighted (T1w) images were acquired using three-dimensional (3D) magnetization-prepared 180° radio-frequency pulses and rapid gradient-echo (MP-RAGE) sequence (repetition time: 2500 ms, echo time: 2.82 ms, flip angle: 7°, TI = 1100 ms, GRAPPA factor = 2, 1.0 mm³ isotropic voxels, 192 contiguous sagittal slices). The DMI sequence was acquired using the following parameters: axial orientation, 42 slices; voxel size, 1.5 × 1.5 × 3 mm³; repetition time = 2800 ms; echo time = 88 ms; bandwidth, 1778 Hz; flip angle, 90°; simultaneous multiband acceleration factor, 2; GRAPPA factor, 2, 58 diffusion-encoding gradient directions, 15 nondiffusion-weighted images, 2 × 58 images with *b*-factors 1000 and 2000 s/mm²; acquisition time, 6 minutes, 22 seconds.

Calculation of DMI Parameters

Data processing was implemented within our in-house postprocessing platform NORA (www.nora-imaging.org) and performed as previously described.¹⁸ In short, preprocessing of diffusion-weighted images included a denoising step²⁴ followed by correction of the Gibbs-ringing artifacts²⁵ and upsampling to an isotropic resolution of 1.5 mm³. Microstructural diffusion metrics were estimated using a Bayesian approach¹⁵

that determines the three components of a WM-based tissue^{15,16}: (1) the free-fluid/CSF fraction (V-CSF) in which molecules randomly move at the distance of their diffusion length (in the range of a tenth of a micrometer); (2) the volume fraction within neuronal processes (ie, axons and dendrites; V-intra) with almost one-dimensional molecule diffusion due to tight membrane borders; and (3) the volume fraction outside of axons or dendrites (V-extra), characterized by an intermediate constraint to molecule diffusion representing the cellular compartment and the extracellular matrix. Although primarily developed for WM, multicompartiment dMRI metrics have been employed to investigate gray matter (GM) also.^{19,26} T1w imaging datasets were spatially normalized using CAT12 (<http://www.neuro.uni-jena.de/cat/>), and dMRI images were coregistered to the T1w images. Validity of coregistration between dMRI and T1w images was manually confirmed. Further quality control was performed by visually inspecting each individual DMI map.

Region-of-Interest-Based Analysis

To investigate the microstructure in pathognomonic localizations in MSA, a region-of-interest (ROI) based approach was employed. MSA mainly affects the putamen, SN, dentate nucleus, and cerebellar cortex.² We assessed the microstructure in gray and WM regions in both the cerebellopontine and the nigrostriatal systems. Regarding the cerebellar cortex, there is a high risk of partial volume effects with CSF in the readout, whereas the dentate nucleus is a rather small structure that one might speculate about substantial partial volume effects even in healthy subjects.²⁷ We thus chose to assess the interconnecting WM tracts MCP and PCT²⁸ in addition to the dentate nucleus²⁷ while omitting the cerebellar cortex. For the nigrostriatal system, we assessed the SN,²⁹ the putamen, and the nigrostriatal tract. We chose expert reader manual segmentations for the putamen to exclude the parameter extraction of adjacent structures, as automated atlas-based approaches were impaired due to severe MSA-related atrophy. From our point of view, this is crucial because pronounced macroatrophy,³⁰ especially of the putamen, can lead to incorrect segmentation of the ROIs using approaches such as probabilistic atlases or FreeSurfer and, thus limiting the assessment of the microstructural changes. The nigrostriatal tract was defined in a global tractography approach—details are provided in Data S1 (Fig S1). The atlas-derived ROIs and the one for the nigrostriatal tract were not altered and diffeomorphically warped from Montreal Neurological Institute (MNI) space to the individual patient's space. DMI metrics for the cerebellopontine and nigrostriatal ROIs were extracted from brain parenchyma voxels only, so as to address partial volume effects due to atrophy as well.²⁷⁻²⁹ For

this purpose, DMI metrics were read only from voxels with gray or WM tissue probability value >0.6, as obtained using CAT12. Similarly, as widespread microstructural alteration in MSA is known,³¹ we investigated two control ROIs in the gray (superior temporal gyrus³²) and WM (superior parietal WM²⁸).

Statistical Analysis

Statistical analyses were performed using R (version 4.1.0, <https://www.R-project.org/>). Data are presented as the mean and standard deviation for continuous variables, and as absolute frequencies and percentages for categorical variables. The Shapiro–Wilk test was used to assess normal distribution of data. We compared the demographic and clinical characteristics of patient and control groups using analysis of variance followed by Tukey's honest significance test or χ^2 test when applicable. Between-group differences of DMI parameters were assessed using age- and sex-adjusted analysis of covariance, followed by Tukey's honest significance test. We estimated the effect sizes for pairwise comparisons using Cohen's *d*. Partial Spearman's correlations controlling for age and sex (R package *ppcor*)³³ were used to test the strength of the relationship between the time to solve 9HPB and DMI parameters in the respective ROIs. Because all analyses were exploratory in nature, *P*-values were not corrected for multiple comparisons. The significance threshold was set to *P* < 0.05.

Code Availability

The R code used in our analysis is available from the corresponding author on reasonable request.

Results

Participants

There were no group differences in terms of sex between HCs and patients with MSA-P (χ^2 , *P* = 0.178) or MSA-C (*P* = 0.320), whereas patients with MSA-P and MSA-C differed in terms of sex (*P* = 0.016). No differences were observed in terms of age between the HCs and patients with MSA-P (*P* = 0.255) or MSA-C (*P* = 0.365), whereas patients with MSA-C were younger than those with MSA-P (*P* = 0.020). Demographic and clinical data are presented in Table 1. Performance in 9HPB was below the respective cutoff in 31 of 33 patients with MSA-P and 8 of 10 patients with MSA-C, indicating impaired dexterity. For more detailed information and reference values, see Table 2.²⁸

TABLE 1 Demographics and clinical characteristics of the MSA patient group

	Controls (N = 31)	MSA-P (N = 47)	MSA-C (N = 17)
Sex			
Female	17 (54.8%)	34 (72.3%)*	6 (35.3%)*
Male	14 (45.2%)	13 (27.7%)	11 (64.7%)
Age at imaging (y)			
Mean (SD)	63.6 (9.25)	65.8 (8.40)	64.5 (7.02)
Disease duration at imaging (y)			
Mean (SD)		3.87 (2.09)	3.09 (1.85)
Time to solve 9-Hole Peg Board (s)			
Mean (SD)		40.5 (16.0)	37.1 (9.8)

Note: Time to solve the 9-Hole Peg Board was available in $n = 10$ patients with MSA-C and $n = 33$ patients with MSA-P. *Indicates a significant intergroup difference ($P = 0.023$), whereas all other intergroup comparisons were not statistically significant ($P > 0.05$).

Abbreviations: MSA, multiple system atrophy; MSA-P, multiple system atrophy-parkinsonian subtype; MSA-C, multiple system atrophy-cerebellar dysfunction subtype; SD, standard deviation.

ROI-Based Group Comparison of DMI Parameters in the Nigrostriatal and Cerebellopontine Systems

DMI parameters were compared between patients with MSA-P and MSA-C and HCs after extraction from the putamen based on expert segmentation and from the SN, nigrostriatal tract, dentate nucleus, MCP, and PCT via atlas-derived ROIs.^{28,29} Here, the putaminal free-fluid fraction was larger in patients with MSA-P than in HCs ($P < 0.001$, $t = 8.53$, $d = -1.95$) and those with MSA-C ($P < 0.001$, $t = 4.09$, $d = -1.21$) as well as larger in patients with MSA-C than in HCs ($P = 0.024$, $t = 2.66$, $d = -1.05$). This was corroborated by a decrease in the extra-neurite cellular compartment that was lower in patients with MSA-P than in HCs ($P < 0.001$, $t = -7.45$, $d = 1.71$), or in those with MSA-C ($P = 0.010$, $t = -4.41$, $d = 1.15$), with no significant differences between MSA-C patients and HCs ($P = 0.135$, $t = -1.93$,

$d = 0.71$). No alterations were observed in the intra-axonal and dendritic compartment (Fig. 2). This pattern is consistent with a neurodegenerative loss of cells.¹⁹

Nigral free-fluid fraction was significantly larger in MSA-P (V-CSF, $P < 0.001$, $t = 6.22$, Cohen's $d = -1.47$) and MSA-C patients ($P < 0.001$, $t = 3.85$, $d = -1.42$) compared to HCs, with no difference between the MSA subtypes. Correspondingly, a decrease in V-extra was observed in patients with MSA-P compared to those with MSA-C ($P = 0.035$, $t = -2.525$, $d = 0.38$) and HCs ($P = 0.002$, $t = -3.60$, $d = 0.71$), but no difference was observed between patients with MSA-C and HCs. Additionally, no significant group differences in the intra-axonal and dendritic compartment were observed (Fig. 2). As in the case of the putamen, these changes are consistent with a neurodegenerative loss of cells.

In the nigrostriatal tract, we observed a larger free-fluid fraction in patients with MSA-P than in HCs ($P < 0.001$, $t = 5.52$, $d = -1.26$) and at trend level MSA-C ($P = 0.055$, $t = 2.34$, $d = -0.48$), with no

TABLE 2 Age-adjusted 9-Hole Peg Board reference values and frequency of impaired performance in MSA-P and MSA-C

Age (y)	Reference male (s)	Reference female (s)	MSA-P impaired in 9HPB performance	MSA-C impaired in 9HPB performance
45–49	20 + 3	18 ± 2	1/1	
50–54	20 + 2	19 ± 3	1/2	1/1
55–59	20 + 3	19 + 2	4/4	2/2
60–64	21 + 3	20 + 2	7/7	1/2
65–69	22 + 3	21 + 3	9/10	3/3
70–74	23 + 4	21 + 3	5/5	1/1
>74	25 + 4	23 + 3	4/4	0/1
Total			–31/33	8/10

Abbreviations: MSA-P, multiple system atrophy-parkinsonian subtype; MSA-C, multiple system atrophy-cerebellar dysfunction subtype; 9HPB, 9-Hole Peg Board.

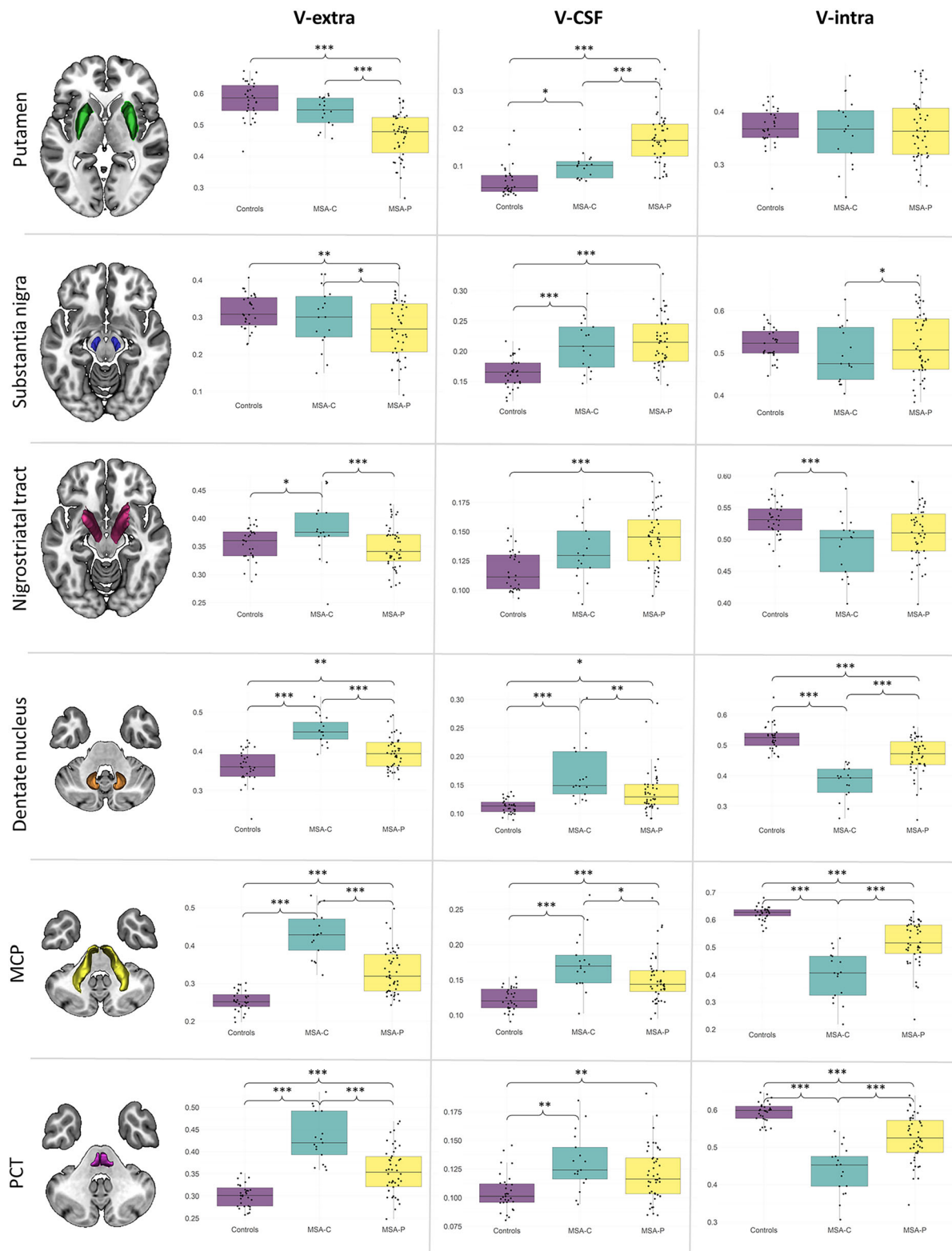


FIG. 2. Group comparisons of microstructural compartments (V-extra, V-CSF, and V-intra) in the putamen, substantia nigra, nigrostriatal tract, dentate nucleus, middle cerebellar peduncle (MCP), and pontine crossing tract (PCT) between HC (healthy control), MSA-P (multiple system atrophy-parkinsonian subtype) and MSA-C (multiple system atrophy-cerebellar subtype) groups. Dots represent individual subject values, and boxplots show group median, quartiles, and minimum and maximum values. Significance threshold: * $P < 0.05$, ** $P < 0.01$, and *** $P < 0.001$. [Color figure can be viewed at wileyonlinelibrary.com]

significant difference between patients with MSA-C and HCs ($P = 0.112$, $t = 2.02$, $d = -0.77$). The extra-neurite cellular compartment (V-extra) was larger in patients with MSA-C than in those with MSA-P ($P < 0.001$, $t = -4.01$, $d = 0.75$) and HCs ($P = 0.015$, $t = 2.84$, $d = -0.66$), and no differences were found between patients with MSA-P and HCs ($P = 0.374$, $t = -1.34$, $d = -0.16$). These changes were accompanied by a decrease in the intra-axonal and dendritic compartment (V-intra) that was smaller in patients with MSA-C than in those with MSA-P ($P = 0.032$, $t = 2.55$, $d = -0.45$) and HCs ($P < 0.001$, $t = -3.83$, $d = 1.13$), and no differences were found between patients with MSA-P and HCs ($P = 0.192$, $t = -1.75$, $d = 0.57$).

We observed a distinct pattern of microstructural alterations within the cerebellopontine WM regions. In detail, the free-fluid fraction in the MCP was larger in MSA-P patients than in HCs ($P < 0.001$, $t = 3.92$, $d = -1.05$) but lower than in the MSA-C group ($P = 0.035$, $t = -2.52$, $d = 0.61$) as well as larger in MSA-C patients than in HCs ($P < 0.001$, $t = 5.49$, $d = -1.93$). The cellular compartment was larger in patients with MSA-P compared to HCs ($P < 0.001$, $t = 6.14$, $d = -1.60$) but smaller than in patients with MSA-C ($P < 0.001$, $t = -7.05$, $d = 1.61$) as well as larger in patients with MSA-C than in HCs ($P < 0.001$, $t = 11.60$, $d = -4.17$).

In contrast to the GM structures SN and putamen (with no significant volume shifts in V-intra), MCP V-intra was smaller in patients with MSA-P compared to HCs ($P < 0.001$, $t = -6.21$, $d = 1.66$) but larger than in patients with MSA-C ($P < 0.001$, $t = 6.23$, $d = -1.41$) as well as smaller in MSA-C patients compared to HCs ($P < 0.001$, $t = -10.86$, $d = 3.97$). In analogy to MCP, the free-fluid fraction in PCT was larger in patients with MSA-P than in HCs ($P = 0.004$, $t = 3.29$, $d = -0.75$) but not different from that in patients with MSA-C ($P = 0.451$) as well as larger in patients with MSA-C than in HCs ($P = 0.001$, $t = 3.72$, $d = -1.33$). The cellular compartment was larger in patients with MSA-P compared to HCs ($P < 0.001$, $t = 4.72$, $d = -1.25$) but smaller than in MSA-C ($P < 0.001$, $t = -6.98$, $d = 1.41$) as well as larger in patients with MSA-C than in HCs ($P < 0.001$, $t = 10.42$, $d = -3.37$). Similar to MCP, in PCT the intra-axonal volume fraction was reduced in patients with MSA-P compared to HCs ($P < 0.001$, $t = -5.21$, $d = 1.39$) but larger than in patients with MSA-C ($P < 0.001$, $t = 6.23$, $d = -1.37$) as well as smaller in patients with MSA-C compared to HCs ($P < 0.001$, $t = -10.08$, $d = 3.56$). This is consistent with the loss of cerebellopontine axonal fibers (Fig. 2).

We observed a larger free-fluid (V-CSF) fraction in the dentate nucleus in patients with MSA-C than in those with MSA-P ($P = 0.005$, $t = -3.21$, $d = 0.73$)

and HCs ($P < 0.001$, $t = 5.36$, $d = -1.82$), and in patients with MSA-P compared with HCs ($P = 0.013$, $t = 2.90$, $d = -0.84$). Similarly, the extra-neurite cellular compartment (V-extra) was larger in patients with MSA-C than in those with MSA-P ($P < 0.001$, $t = -4.58$, $d = 1.42$) and HCs ($P < 0.001$, $t = 7.25$, $d = -2.24$) and larger in patients with MSA-P than HCs ($P = 0.001$, $t = 3.63$, $d = -0.84$). These changes were accompanied by a decrease in the intra-axonal and dendritic compartment (V-intra) that was smaller in patients with MSA-C than in those with MSA-P ($P < 0.001$, $t = 5.50$, $d = -1.47$) and HCs ($P < 0.001$, $t = -8.85$, $d = 3.16$) as well as in patients with MSA-P compared with HCs ($P < 0.001$, $t = -4.55$, $d = 1.11$).

Regarding the control regions, no statistical group differences were observed in either compartment in the superior temporal GM ($P > 0.05$). However, free-fluid fraction (V-CSF) in the superior parietal WM was larger in patients with MSA-P than in HCs ($P = 0.062$, $t = 2.29$, $d = -0.54$) at trend level, with no differences between patients with MSA-P and MSA-C ($P = 0.848$) and those with MSA-C and HCs ($P = 0.423$). Extra-neurite and cellular compartment (V-extra) was lower in patients with MSA-C than in HCs ($P = 0.017$, $t = 2.78$, $d = -0.84$), with no intergroup differences between patients with MSA-C and MSA-P ($P = 0.178$) as well as those with MSA-P and HCs ($P = 0.367$). Additionally, we observed a smaller intra-axonal and dendritic compartment (V-intra) in patients with MSA-C ($P = 0.005$, $t = -3.20$, $d = 1.01$) and MSA-P ($P = 0.034$, $t = -2.52$, $d = 0.58$) compared with HCs, with no differences between MSA-C and MSA-P ($P = 0.411$) (Fig. S2).

As revealed in the ROI-based analyses and shown in Figure 2, GM alterations of V-CSF and V-extra represent the same process, only with opposite directions of effect. This was reflected by a negative Pearson's correlation coefficient between V-CSF and V-extra in putamen ($R = -0.82$, $P < 0.001$). However, in WM, a shift was observed from the intra- to the extra-axonal and free-fluid compartments. Again, this was reflected by a negative Pearson's correlation coefficient between V-intra and V-CSF ($R = -0.84$, $P < 0.001$). Though established in assessing GM microstructure, the standard model rather relies on WM mesostructure.¹⁴⁻¹⁶ As the parameter V-CSF is most stable in GM,¹⁵ all analyses were confined to V-CSF in GM and V-intra in WM structures.

Analysis of the Association between Nigrostriatal and Cerebellar Microstructures and Dexterity in MSA-P and MSA-C

Time to solve 9HPB was pathologic in 31 of 33 patients with MSA-P and in 8 of 10 patients with MSA-C and did not differ between both subtypes

($P = 0.520$).²³ In MSA-P, time to solve 9HPB was not associated with either putaminal ($\rho = -0.204$, $P = 0.270$) or nigral free fluid ($\rho = 0.230$, $P = 0.213$), and no association between the axonal volume fraction and nigrostriatal tract was observed ($\rho = -0.28$, $P = 0.125$). However, an association was observed between the time to solve 9HPB and the axonal volume fraction of MCP ($\rho = -0.404$, $P = 0.024$) and PCT ($\rho = -0.517$, $P = 0.003$) as well as the free-fluid compartment in the dentate nucleus ($\rho = 0.42$, $P = 0.018$). A similar pattern was found in MSA-C where no association between time to solve 9HPB and putaminal ($\rho = -0.011$, $P = 0.980$) or nigral ($\rho = -0.341$, $P = 0.408$) axonal volume fraction was observed, contrasted by an association between the time to solve 9HPB and the axonal volume fraction of MCP ($\rho = -0.733$, $P = 0.038$) and PCT ($\rho = -0.745$, $P = 0.034$). However, no association was observed between the free-fluid fraction of the dentate nucleus ($\rho = 0.55$, $P = 0.157$) (Fig. S3). The associations observed in the two subgroups of MSA persisted when they were combined into a complete MSA group (Table 3). The full set of correlations between nigrostriatal and cerebellopontine ROI-derived DMI metrics and dexterity is provided in Table 3.

Of note, no associations between dexterity and the control ROIs in the gray and WM were found (Fig. S2).

Discussion

DMI revealed nigrostriatal and cerebellar neurodegeneration in MSA with a distinct accentuation for the two subtypes. In the nigrostriatal GM regions (ie, the SN and putamen), an increase in the interstitial free fluid (V-CSF) was accompanied by cellular degeneration, as reflected by a decrease in V-extra. In contrast, axonal degeneration was detected in the cerebellopontine WM tracts (ie, PCT and MCP) by a decrease in V-intra. Axonal degeneration with reduced V-intra and increased V-CSF was found in the nigrostriatal tract, and also in the dentate nucleus, we observed a strong decrease in the axonal compartment with a concomitant increase in the free fluid. Regarding the Parkinson subtype, a strong putaminal accentuation was observed, whereas in MSA-C, a cerebellar pattern was predominant. Moreover, cerebellopontine (but not nigrostriatal) degeneration was associated with impaired dexterity in both subtypes.

Microstructural dMRI techniques have previously been employed to investigate putaminal degeneration in MSA-P. Using the bicompartamental free water imaging approach, elevated nigral free fluid was observed in MSA compared to HCs.³⁴ Extending this, a recent NODDI-based study observed putaminal increases in the cellular compartment (Vic) and free fluid (Viso)

with simultaneous decreases in the orientation dispersion index (ODI).³⁵ In contradiction to this latter work, we observed a significant increase in putaminal free fluid paralleled by a significant decrease in the somata fraction, analogous to SN. This effect persisted in both subtypes but was more pronounced in MSA-P than in MSA-C.

Regarding the SN, several studies employed advanced dMRI techniques and observed elevated nigral free fluid with ($n = 31$ MSA-P³¹) and without ($n = 21$ MSA-P³⁵) alterations in the intracellular volume fraction. In line with these findings, we observed more nigral free fluid in patients with MSA-P when compared to HCs, though we furthermore found a decrease in the somata-associated fraction (V-extra). Similarly, elevated nigral free fluid was observed in patients with MSA-C. However, the cellular fraction was slightly reduced when compared to that in patients with MSA-P with only a small effect size, contrasting with the large effects observed in the putamen. These findings of GM neurodegeneration are corroborated by the axonal degeneration we noted in the interconnecting nigrostriatal tract.

In the WM tracts MCP and PCT, we found evidence of axonal degeneration through a reduction in the axonal compartment that was more pronounced in MSA-C than MSA-P. This was accompanied by a strong increase in the free interstitial fluid. With respect to the increased free fluid, partial neuroinflammation is conceivable as well, because this has also been described in MSA alongside neurodegeneration,³⁶ and both neuroinflammation¹⁸ and neurodegeneration¹⁹ can lead to increased interstitial fluid. The similar pattern of parameter alterations in the GM area of the dentate nucleus can be attributed to the fact that the efferent axons in the dentate nucleus hilus constitute a substantial proportion of the ROI.³⁷ We have thus rather indirectly demonstrated the degeneration of this GM region. However, the validity of these alterations in DMI parameters is supported both by the accentuation in the MSA-C cohort and by the strong association with dexterity.

Our findings regarding the WM regions nigrostriatal tract, MCP, and PCT are in line with a previous study that observed a reduction in cellular and myelin volume fraction, accompanied by elevated free fluid in MSA-P.³¹ However, in contrast to this study, we observed a relative increase in V-extra. This can be explained by two mechanisms: (1) V-extra in the WM contains the extracellular matrix, which indicates gliosis as observed in both MSA subtypes²; or (2) only a relative increase in this fraction is present due to a drastic decrease in the axonal fraction as the formerly largest volume fraction in HCs in these tracts. Moreover, the observed microstructural alterations (with different accentuations in MSA-P and MSA-C) reflect known macrostructural atrophy of the putamen or cerebellum.³⁰

TABLE 3 Partial Spearman's correlations between DMI metrics and 9-Hole Peg Board performance of nigrostriatal and cerebellopontine regions

ROI	MSA-P			MSA-C			MSA-P and MSA-C combined		
	V-extra	V-CSF	V-intra	V-extra	V-CSF	V-intra	V-extra	V-CSF	V-intra
Putamen	$\rho = 0.27$ $P = 0.136$	$\rho = -0.20$ $P = 0.270$	$\rho = -0.19$ $P = 0.307$	$\rho = 0.11$ $P = 0.786$	$\rho = -0.01$ $P = 0.980$	$\rho = 0.06$ $P = 0.881$	$\rho = 0.09$ $P = 0.570$	$\rho = 0.03$ $P = 0.853$	$\rho = -0.14$ $P = 0.398$
Substantia nigra	$\rho = 0.19$ $P = 0.293$	$\rho = 0.23$ $P = 0.213$	$\rho = -0.28$ $P = 0.129$	$\rho = -0.07$ $P = 0.876$	$\rho = -0.34$ $P = 0.408$	$\rho = 0.26$ $P = 0.529$	$\rho = 0.10$ $P = 0.53$	$\rho = 0.11$ $P = 0.483$	$\rho = -0.17$ $P = 0.280$
Nigrostriatal tract	$\rho = 0.30$ $P = 0.107$	$\rho = 0.03$ $P = 0.886$	$\rho = -0.28$ $P = 0.125$	$\rho = 0.51$ $P = 0.195$	$\rho = -0.33$ $P = 0.423$	$\rho = -0.47$ $P = 0.237$	$\rho = 0.26$ $P = 0.099$	$\rho = 0.01$ $P = 0.926$	$\rho = -0.26$ $P = 0.096$
Dentate nucleus	$\rho = 0.39$ $P = 0.030$	$\rho = 0.42$ $P = 0.018$	$\rho = -0.56$ $P = 0.001$	$\rho = 0.34$ $P = 0.407$	$\rho = 0.55$ $P = 0.157$	$\rho = -0.88$ $P = 0.004$	$\rho = 0.27$ $P = 0.083$	$\rho = 0.38$ $P = 0.013$	$\rho = -0.43$ $P = 0.006$
Middle cerebellar peduncle	$\rho = 0.43$ $P = 0.017$	$\rho = 0.19$ $P = 0.300$	$\rho = -0.40$ $P = 0.024$	$\rho = 0.70$ $P = 0.051$	$\rho = 0.63$ $P = 0.095$	$\rho = -0.73$ $P = 0.038$	$\rho = 0.34$ $P = 0.030$	$\rho = 0.26$ $P = 0.100$	$\rho = -0.35$ $P = 0.024$
Pontine crossing tract	$\rho = 0.42$ $P = 0.019$	$\rho = 0.45$ $P = 0.011$	$\rho = -0.517$ $P = 0.003$	$\rho = 0.73$ $P = 0.039$	$\rho = 0.63$ $P = 0.094$	$\rho = -0.75$ $P = 0.034$	$\rho = 0.32$ $P = 0.037$	$\rho = 0.49$ $P = 0.001$	$\rho = -0.43$ $P = 0.005$

Abbreviations: DMI, diffusion microstructure imaging; ROI, region of interest; MSA-P, multiple system atrophy-parkinsonian subtype; MSA-C, multiple system atrophy-cerebellar dysfunction subtype.

Therefore, in conjunction with the nigrostriatal degeneration discussed earlier, a conceivable explanation arises: whereas degeneration accentuated in the putamen leads to MSA-P, prominent cerebellopontine degeneration (as captured by MCP as well as its crossing portion within PCT) leads to MSA-C, and nigral degeneration is common to both diseases. The fact that the changes in the regions investigated have the same direction of effect in both subtypes supports the hypothesis (underpinned neuropathologically and with dMRI data) on MSA as a single entity with the two subtypes at the edges of a spectrum.^{38,39} This is further corroborated by the association between microstructure and the performance in 9HPB in both subtypes.

Having initially elaborated that DMI is able to detect neurodegenerative changes in MSA and that these differ between the two subtypes, we then investigated the extent to which there is a relationship with dexterity. Substantial impairment in dexterity was observed in both MSA-C and MSA-P, with similar impairment in both subtypes. In patients with MSA-P, one might expect that dexterity would (1) be primarily caused by nigrostriatal degeneration and (2) constitute a part of the Parkinson's syndrome. Interestingly, we did not find an association between time to solve the 9HPB and nigrostriatal degeneration but instead a strong association with the degeneration of the cerebellopontine system. In MSA-C, a similar association was observed in our cohort. This finding is of special interest as it provides a more profound insight into the neurodegenerative origin of clinical impairment of patients with MSA. Of note, although no significant association between impaired dexterity and the free-fluid compartment of the dentate nucleus was observed, we observed a strong association with the intra-axonal compartment, indicating that the demise of efferent fibers contributes to impaired dexterity and might be even more relevant than the degeneration of the somata. In addition to a better understanding of the disease, this has practical implications as the benefit of specific physiotherapy in patients with cerebellar degeneration is well known.^{40,41} To further validate these results, we examined these associations in a cohort comprising both subtypes, in which we observed similar effects. This further corroborates the hypothesis that MSA-P and MSA-C represent different ends on a continuum of the same disease entity.

In accordance with our findings, a recent study conducted by Wilkes and colleagues reported an association between peg board performance and the superior cerebellar peduncle, which is consistent with our results. However, contrary to the outcomes of our study, they observed a relationship between dexterity and the nigrostriatal tract. This contradiction is primarily explained by the fact that our study evaluated patients with MSA-P and MSA-C separately, whereas

the other study examined a combined group of individuals with atypical Parkinson's syndromes, comprising 33 patients with progressive supranuclear palsy and 23 with MSA.⁴²

The retrospective nature of our study displays a limitation because it led to incomplete datasets limiting the possibility for assessing the association between individual symptoms and distinct neurodegenerative alterations. Nevertheless, we assume that the observations are sufficiently supported by the available data points on the 9HPB (present in 70% of the MSA-P and 59% of the MSA-C), as a concise pattern of association with cerebellar neurodegeneration was evident across both groups. Further, postmortem diagnoses were lacking. In addition, because the diagnosis of MSA poses a major challenge in clinical routine practice with a diagnostic accuracy of 60%,⁴³ patients with disorders other than MSA might have been erroneously included in this study. However, diagnoses were carefully validated by three experts in movement disorders based on the current diagnostic consensus criteria,¹ and [¹⁸F]FDG-PET²¹ was available in all patients, supportive of the respective clinical diagnosis. In contrast, our study has major strengths. First, the case numbers for both subgroups are relatively large. Second, in contrast to previous studies, the association between cerebral microstructure and clinical parameters was assessed using partial correlations, controlling for age and sex, given the impact of these on cerebral microstructure.⁴⁴

In summary, our analysis of a large and clinically representative cohort of patients with MSA-P and MSA-C revealed a common neurodegenerative pattern in both subtypes with putaminal-accentuated degeneration in MSA-P, whereas cerebellar-accentuated degeneration was associated with MSA-C. Furthermore, we observed an association between dexterity and cerebellar but not nigrostriatal degeneration in both MSA-C and MSA-P. This indicates that cerebellar dysfunction is functionally relevant and disabling in patients with MSA-P also. Nigrostriatal and cerebellar integrity are promising biomarkers for possible disease-modifying studies and individualized therapies. ■

Acknowledgments: Alexander Rau was supported by Berta-Ottenstein-Programme for Clinician Scientists, Faculty of Medicine, University of Freiburg. Open Access funding enabled and organized by Projekt DEAL.

Data Availability Statement

The dataset is available from the corresponding author upon reasonable request and approval by the local ethics committee.

References

1. Wenning GK, Stankovic I, Vignatelli L, Fanciulli A, Calandra-Buonaura G, Seppi K, et al. The Movement Disorder Society criteria for the diagnosis of multiple system atrophy. *Mov Disord* 2022; 37(6):1131–1148.
2. Ozawa T, Paviour D, Quinn NP, Josephs KA, Sangha H, Kilford L, et al. The spectrum of pathological involvement of the striatonigral and olivopontocerebellar systems in multiple system atrophy: clinicopathological correlations. *Brain* 2004;127(12):2657–2671.
3. Tu P h, Galvin JE, Baba M, Giasson B, Tomita T, Leight S, et al. Glial cytoplasmic inclusions in white matter oligodendrocytes of multiple system atrophy brains contain insoluble α -synuclein. *Ann Neurol* 1998;44(3):415–422.
4. Fanciulli A, Wenning GK. Multiple-system atrophy. *N Engl J Med* 2015;372(3):249–263.
5. Roncevic D, Palma JA, Martinez J, Goulding N, Norcliffe-Kaufmann L, Kaufmann H. Cerebellar and parkinsonian phenotypes in multiple system atrophy: similarities, differences and survival. *J Neural Transm* 2014;121(5):507–512.
6. Xiao Y, Zhang L, Wei Q, Ou R, Hou Y, Liu K, et al. Health-related quality of life in patients with multiple system atrophy using the EQ-5D-5L. *Brain Behav* 2022;12(10):e2774.
7. Wenning GK, Tison F, Seppi K, Sampaio C, Diem A, Yekhelef F, et al. Development and validation of the unified multiple system atrophy rating scale (UMSARS). *Mov Disord* 2004;19(12):1391–1402.
8. Yang CJ, Hsu HY, Lu CH, Chao YL, Chiu HY, Kuo LC. The associations among hand dexterity, functional performance, and quality of life in diabetic patients with neuropathic hand from objective- and patient-perceived measurements. *Qual Life Res* 2015;24(1):213–221.
9. Feys P, Lamers I, Francis G, Benedict R, Phillips G, LaRocca N, et al. The nine-hole peg test as a manual dexterity performance measure for multiple sclerosis. *Mult Scler* 2017;23(5):711–720.
10. Rimmele DL, Frey BM, Cheng B, Schulz R, Krawinkel LA, Bönstrup M, et al. Association of Extrapyramidal Tracts' integrity with performance in fine motor skills after stroke. *Stroke* 2018; 49(12):2928–2932.
11. Kamagata K, Zalesky A, Hatano T, Ueda R, Di Biase MA, Okuzumi A, et al. Gray matter abnormalities in idiopathic Parkinson's disease: evaluation by diffusional kurtosis imaging and neurite orientation dispersion and density imaging. *Hum Brain Mapp* 2017;38(7):3704–3722.
12. Canu E, Agosta F, Riva N, Sala S, Prella A, Caputo D, et al. The topography of brain microstructural damage in amyotrophic lateral sclerosis assessed using diffusion tensor MR imaging. *AJNR Am J Neuroradiol* 2011;32(7):1307–1314.
13. Bai X, Guo T, Chen J, Guan X, Zhou C, Wu J, et al. Microstructural but not macrostructural cortical degeneration occurs in Parkinson's disease with mild cognitive impairment. *npj Parkinsons Dis*. 2022;8(1):1–9.
14. Zhang H, Schneider T, Wheeler-Kingshott CA, Alexander DC. NODDI: practical in vivo neurite orientation dispersion and density imaging of the human brain. *Neuroimage* 2012;61(4):1000–1016.
15. Reisert M, Kellner E, Dhital B, Hennig J, Kiselev VG. Disentangling micro from mesostructure by diffusion MRI: a Bayesian approach. *Neuroimage* 2017;147:964–975.
16. Novikov DS, Jensen JH, Helpert JA, Fieremans E. Revealing mesoscopic structural universality with diffusion. *Proc Natl Acad Sci U S A* 2014;111(14):5088–5093.
17. Demerath T, Donkels C, Reisert M, Heers M, Rau A, Schröter N, et al. Gray-white matter blurring of the temporal pole associated with hippocampal sclerosis: a microstructural study involving 3 T MRI and ultrastructural histopathology. *Cereb Cortex* 2021;32(9):1882–1893.
18. Rau A, Schroeter N, Blazhenets G, Dressing A, Walter LI, Kellner E, et al. Widespread white matter oedema in subacute COVID-19 patients with neurological symptoms. *Brain* 2022;145(9):3203–3213.

19. Schröter N, Rijntjes M, Urbach H, Weiller C, Treppner M, Kellner E, et al. Disentangling nigral and putaminal contribution to motor impairment and levodopa response in Parkinson's disease. *npj Parkinsons Dis*. 2022;8(1):1–8.
20. Rau A, Jost WH, Demerath T, Kellner E, Reisert M, Urbach H. Diffusion microstructure imaging in progressive supranuclear palsy: reduced axonal volumes in the superior cerebellar peduncles, dentato-rubro-thalamic tracts, ventromedial thalami, and frontomesial white matter. *Cereb Cortex* 2022;32(24):5628–5636.
21. Meyer PT, Frings L, Rücker G, Hellwig S. 18F-FDG PET in parkinsonism: differential diagnosis and evaluation of cognitive impairment. *J Nucl Med* 2017;58(12):1888–1898.
22. Haaxma CA, Bloem BR, Overeem S, Borm GF, Horstink MWIM. Timed motor tests can detect subtle motor dysfunction in early Parkinson's disease. *Mov Disord* 2010;25(9):1150–1156.
23. Oxford Grice K, Vogel KA, Le V, Mitchell A, Muniz S, Vollmer MA. Adult norms for a commercially available nine hole peg test for finger dexterity. *Am J Occup Ther* 2003;57(5):570–573.
24. Veraart J, Fieremans E, Novikov DS. Diffusion MRI noise mapping using random matrix theory. *Magn Reson Med* 2016;76(5):1582–1593.
25. Kellner E, Dhital B, Kiselev VG, Reisert M. Gibbs-ringing artifact removal based on local subvoxel-shifts. *Magn Reson Med* 2016;76(5):1574–1581.
26. Genç E, Fraenz C, Schlüter C, Friedrich P, Hossiep R, Voelke MC, et al. Diffusion markers of dendritic density and arborization in gray matter predict differences in intelligence. *Nat Commun* 2018;9(1):1905.
27. Diedrichsen J, Maderwald S, Küper M, Thürling M, Rabe K, Gizewski ER, et al. Imaging the deep cerebellar nuclei: a probabilistic atlas and normalization procedure. *Neuroimage* 2011;54(3):1786–1794.
28. Oishi K, Faria A, Jiang H, Li X, Akhter K, Zhang J, et al. Atlas-based whole brain white matter analysis using large deformation diffeomorphic metric mapping: application to normal elderly and Alzheimer's disease participants. *Neuroimage* 2009;46(2):486–499.
29. Ilinsky I, Horn A, Paul-Gilloteaux P, Gressens P, Verney C, Kultas-Ilinsky K. Human motor thalamus reconstructed in 3D from continuous sagittal sections with identified subcortical afferent territories. *eNeuro [Internet]* 2018;5(3):0060–18.
30. Minnerop M, Specht K, Ruhlmann J, Schimke N, Abele M, Weyer A, et al. Voxel-based morphometry and voxel-based relaxometry in multiple system atrophy—a comparison between clinical subtypes and correlations with clinical parameters. *Neuroimage* 2007;36(4):1086–1095.
31. Ogawa T, Hatano T, Kamagata K, Andica C, Takeshige-Amano H, Uchida W, et al. White matter and nigral alterations in multiple system atrophy-parkinsonian type. *npj Parkinsons Dis* 2021;7(1):1–12.
32. Rolls ET, Huang CC, Lin CP, Feng J, Joliot M. Automated anatomical labelling atlas 3. *Neuroimage* 2020;206:116189.
33. Kim S. Ppcor: an R package for a fast calculation to semi-partial correlation coefficients. *Communications for Statistical Applications and Methods* 2015;22(6):665–674.
34. Planetta PJ, Ofori E, Pasternak O, Burciu RG, Shukla P, DeSimone JC, et al. Free-water imaging in Parkinson's disease and atypical parkinsonism. *Brain* 2016;139(2):495–508.
35. Mitchell T, Archer DB, Chu WT, Coombes SA, Lai S, Wilkes BJ, et al. Neurite orientation dispersion and density imaging (NODDI) and free-water imaging in parkinsonism. *Hum Brain Mapp* 2019;40(17):5094–5107.
36. Gerhard A, Banati RB, Goerres GB, Cagnin A, Myers R, Gunn RN, et al. [11C](R)-PK11195 PET imaging of microglial activation in multiple system atrophy. *Neurology* 2003;61(5):686–689.
37. Yamaguchi K, Goto N. Three-dimensional structure of the human cerebellar dentate nucleus: a computerized reconstruction study. *Anat Embryol* 1997 Sep 1;196(4):343–348.
38. Wang PS, Wu HM, Lin CP, Soong BW. Use of diffusion tensor imaging to identify similarities and differences between cerebellar and parkinsonism forms of multiple system atrophy. *Neuroradiology* 2011;53(7):471–481.
39. Krismer F, Seppi K, Göbel G, Steiger R, Zucal I, Boesch S, et al. Morphometric MRI profiles of multiple system atrophy variants and implications for differential diagnosis. *Mov Disord* 2019;34(7):1041–1048.
40. Ilg W, Synofzik M, Brötz D, Burkard S, Giese MA, Schöls L. Intensive coordinative training improves motor performance in degenerative cerebellar disease. *Neurology* 2009;73(22):1823–1830.
41. Miyai I, Ito M, Hattori N, Mihara M, Hatakenaka M, Yagura H, et al. Cerebellar ataxia rehabilitation trial in degenerative cerebellar diseases. *Neurorehabil Neural Repair* 2012;26(5):515–522.
42. Wilkes BJ, Tobin ER, Arpin DJ, Wang W, et al. Distinct cortical and subcortical predictors of Purdue pegboard decline in Parkinson's disease and atypical parkinsonism. *npj Parkinsons Dis*. 2023;9(1):1–11.
43. Koga S, Aoki N, Uitti RJ, van Gerpen JA, Cheshire WP, Josephs KA, et al. When DLB, PD, and PSP masquerade as MSA: an autopsy study of 134 patients. *Neurology* 2015;85(5):404–412.
44. Kodiweera C, Alexander AL, Harezlak J, McAllister TW, Wu YC. Age effects and sex differences in human brain white matter of young to middle-aged adults: a DTI, NODDI, and q-space study. *Neuroimage* 2016;128:180–192.

Supporting Data

Additional Supporting Information may be found in the online version of this article at the publisher's web-site.